Supplementary Information

Simultaneous Determination of Conductance and Thermopower of Single Molecule Junctions

Jonathan R. Widawsky,[†] Pierre Darancet,[‡] Jeffrey B. Neaton,*[‡] and Latha Venkataraman*[†]

[†]*Department of Applied Physics and Applied Mathematics, Columbia University*
[‡] *Molecular Foundry, Lawrence Berkeley National Laboratory, Berkeley, CA*

Contents:

Measurement, Data Analysis and Additional Data:

STM Break Junction Technique

The conductance of each molecule was measured using the STM-based break-junction technique, where an Au tip (Alfa Aesar, 99.998%) cut to be sharp is brought in and out of contact with a substrate of ~100 nm of gold (Alfa Aesar, 99.999%) evaporated onto cleaved mica disks. The substrate is mounted on a piezoelectric positioner (Mad City Labs), so that sub-angstrom resolution in position is achieved. During the entire break junction procedure, a small, constant bias (10 mV) is applied between the tip and the substrate with a 10kΩ series resistance added in the circuit while the current is measured (Keithley 428-Prog). Piezo control and data collection were performed using a National Instruments PXI Chassis System (with PXI-4461, PXI-6289) at 40 kHz and driven and managed with a custom-program using Igor Pro (Wavemetrics, Inc.).

The experimental set-up is kept under ambient conditions. For each experiment, the substrate is cleaned under UV/Ozone for 15 minutes prior to use. For every conductance trace measurement, the STM tip is first brought into hard contact with the substrate to achieve a conductance greater than ~ 10 G_0. At this point, the junction electrodes are pulled apart at a speed of 15.8 nm/s for 250 ms (or 3.95 nm). Conductance is measured as a function of tip-sample displacement to generate conductance traces. For each tip/substrate pair, at least one set of 1,000 traces of clean gold breaks is collected to ensure the system is clean. Then, the target molecule is deposited by thermal evaporation (by holding the substrate a few cm above liquid phase molecule in ambient conditions) and an additional 1,000 conductance traces are collected. Every molecular conductance trace is binned linearly into conductance bins, without any data selection, and compiled into a single conductance histogram. The conductance histograms for each of the five molecules are given in SI Figure S1. Every molecule was measured using multiple tip/substrate pairs, on different days to check for consistency and reproducibility.

The molecules measured were as follows:

(1) 4,4'-diaminostilbene (Astatech, 97%)
(2) bis-(4-aminophenyl)acetylene (house synthesized)
(3) 1,5-bis(diphenylphospino)pentane (Sigma Aldrich, 97%)
(4) 4,4'-bipyridine (Fluka, 99%)
(5) 1,2-di(4-pyridyl)ethylene (Fluka, 98%)

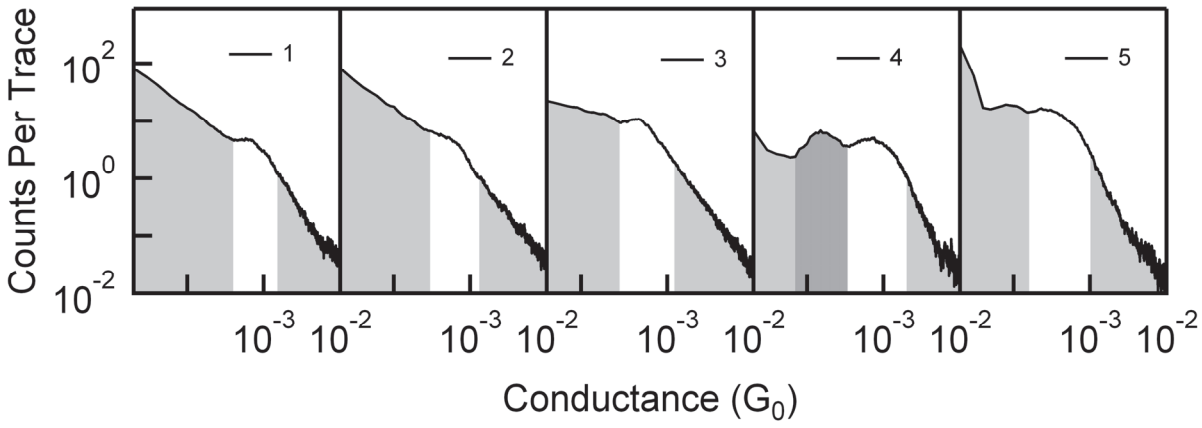

SI Figure S1: Conductance histograms of the five molecules under study. The histograms were each formed from 1000 traces without any sort of data selection using a bin size of 10^{-5} G_0 and are plotted on a log-log scale. The white regions denote the windows used for selection of thermal current measurements. For 4, the dark grey region represents the region of the low-conducting configuration.

For measurement of thermal current, the preceding procedure was modified. A "hold" portion was incorporated into the piezo pull-out ramp, where after the piezo stretched the junction for 2.37 nm, the junction was held constant for 50 ms, and then the stretching continued. During the central two quartiles of the hold (middle 25 ms), the applied bias was dropped to zero, so that all of the current measured here would be due solely to the thermal gradient. The electronics was carefully calibrated to ensure that there were no other sources of bias across the junction after every 1000 measurements. The substrate was mounted onto the hot side of a thermoelectric (Peltier) device, while the cold side was kept near room temperature. Additionally, the STM tip was kept near room temperature throughout the measurement. The temperature of the hot substrate and the tip was recorded using a thermocouple. For each molecule, more than 3600 thermal current traces were collected at each of three ΔT's (0 K, 14 K, 27 K), though not every trace successfully contained a molecular thermal current measurement (i.e. if the gold point contact ruptured "too early" or "too late"). A trace was deemed to successfully measure thermal current through a molecular junction if the average conductance of the first and fourth quartiles of the hold (i.e. when the applied bias is 10 mV) fell within the conductance peak of that respective molecule. The selection regions used are highlighted in white in the conductance histograms in SI Figure S1. The number of traces selected for each molecule at each ΔT is given in the following table.

# Kept Traces	**(1)**	**(2)**	**(3)**	**(4)**	**(5)**
ΔT = 0 K	428	650	528	531	863
ΔT = 14 K	474	581	694	475	682
ΔT = 27 K	410	898	789	1423	956

Histograms of Measured Average Conductance and Thermal Current

The histograms for (**2**) bis-(4-aminophenyl)acetylene, (**3**) 1,5-bis(diphenylphospino)pentane, (**5**) 1,2-di(4-pyridyl)ethylene and (**4**) 4,4'-bipyridine (low conductance geometry), which were not included in the manuscript, are included below (SI Figures S2-S5). In all cases, green denotes $\Delta T = 0$ K, blue denote $\Delta T = 14$ K, and red denotes $\Delta T = 27$ K.

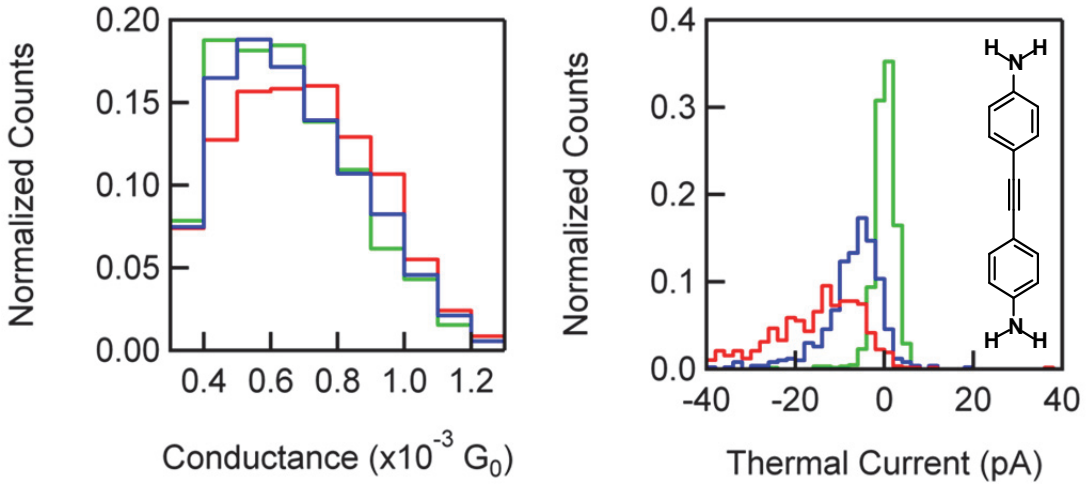

SI Figure S2: Histograms for average conductance (left) and thermal current (right) for (2) for each of the three ΔT's.

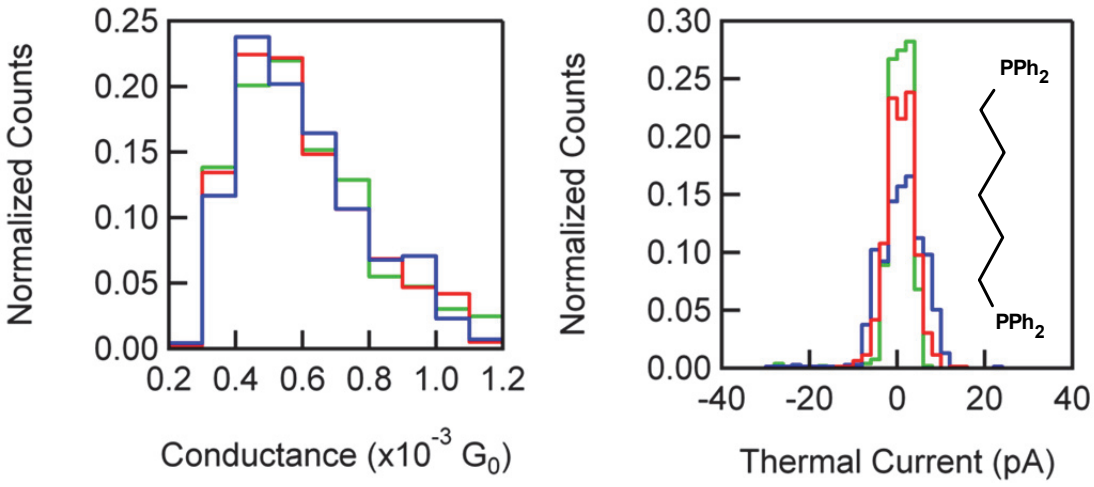

SI Figure S3: Histograms for average conductance (left) and thermal current (right) for (3) for each of the three ΔT's.

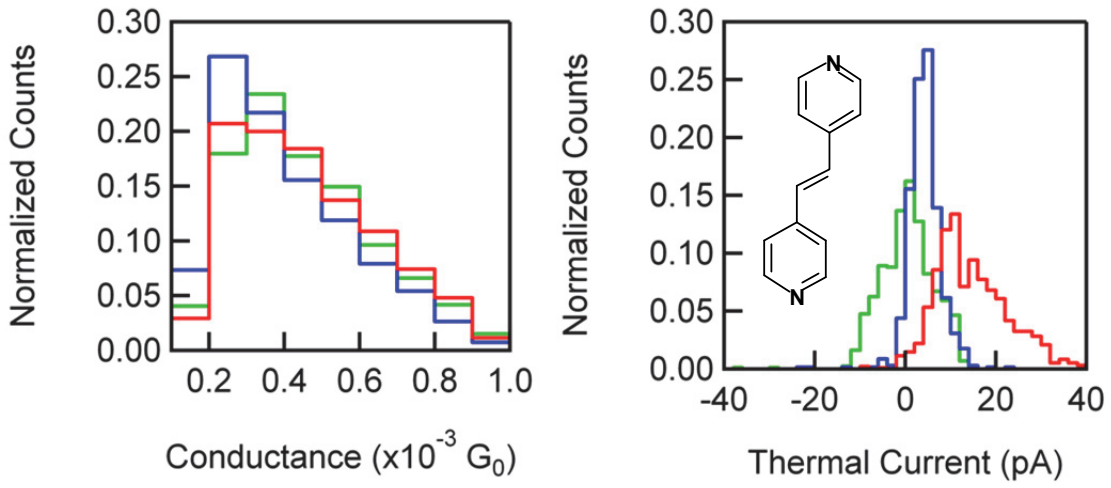

SI Figure S4: Histograms for average conductance (left) and thermal current (right) for (5) for each of the three ΔT's.

Inclusion of the Low-Conducting State of (4) 4,4'-Bipyridine

Although statistics are small, we are also able to obtain a distribution of Seebeck coefficients for junctions with 4,4'-bipyridine in the low-conducting state. The conductance window used is denoted by the dark grey region in the histogram for (**4**) in SI Figure S1. The histograms for thermal current and Seebeck coefficient are given below:

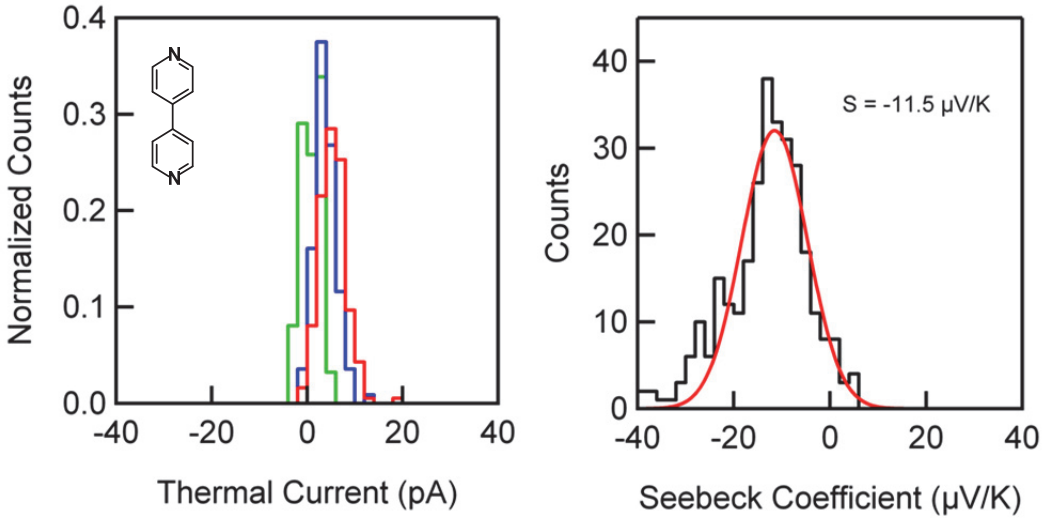

SI Figure S5: Histograms of thermal current (left) at each of the three ΔT's and histogram of molecular Seebeck coefficient (right) for the low-conducting state of 4,4'-bipyridine.

We get a molecular Seebeck coefficient of -11.5 μV/K, which is close to the Seebeck coefficient we get for junctions in the high-conducting state (-9.5 μV/K).

Theoretical Calculations and Additional Data:

First-Principles Optimization of Junction Geometries

We use DFT and the SIESTA package to obtain the self-consistent density with localized numerical orbitals and a 300 Ry grid cutoff, a 0.05 eV electronic smearing, on a 4x4 k-point sampling in directions perpendicular to the junction. The molecules bind preferentially to undercoordinated gold atoms[1, 2]. We examine two different binding motifs and three different junction geometries: one in which the molecule binds to undercoordinated Au atom within a motif consisting of 3 gold adatoms ("Trimer") on both sides; "Trimer-Adatom", where on one side the "Trimer" is replaced with a single adatom binding site; and adatoms on both sides. Hellmann-Feynman forces on the atoms are reduced to 0.04 eV/Å or less using a GGA-PBE functional using double-ζ- basis set. We model our system by 7-layers of 16 gold atoms on both sides, the last 4 layers being constrained to the bulk (PBE) geometry. Initial geometries for molecules (**1**), (**2**), and (**4**) are chosen from previous work on amine- and pyridine-bonded molecules on gold(111)[1-3]. Molecule (**4**) is examined in the high-conductance configuration[1].

Procedures for Transmission and Seebeck Coefficient Calculations

The transmission function is calculated using an energy grid of 100 points between E_F − 5eV and E_F + 5eV, with 100 supplementary points between E_F – 50meV and E_F + 50meV on a 16x16 $k_{||}$ sampling in the directions perpendicular to the junctions, using the Scarlet code[4].

The Seebeck coefficient is calculated taking the best Lorentzian fit with Gnuplot of the transmission function between E_F – 10meV and E_F + 10meV, and then differentiating the Lorentzian analytically.

Position of the molecular levels in DFT

	(1)	**(2)**	**(3)**	**(4)**	**(5)**
HOMO DFT [eV]	-0.73	-0.90	-3.24	-3.41	-2.57
LUMO DFT [eV]	1.80	1.94	3.32	0.28	0.13

Table S1: Energies of the molecular orbitals in DFT with respect to the Fermi level.

DFT Transmission Functions

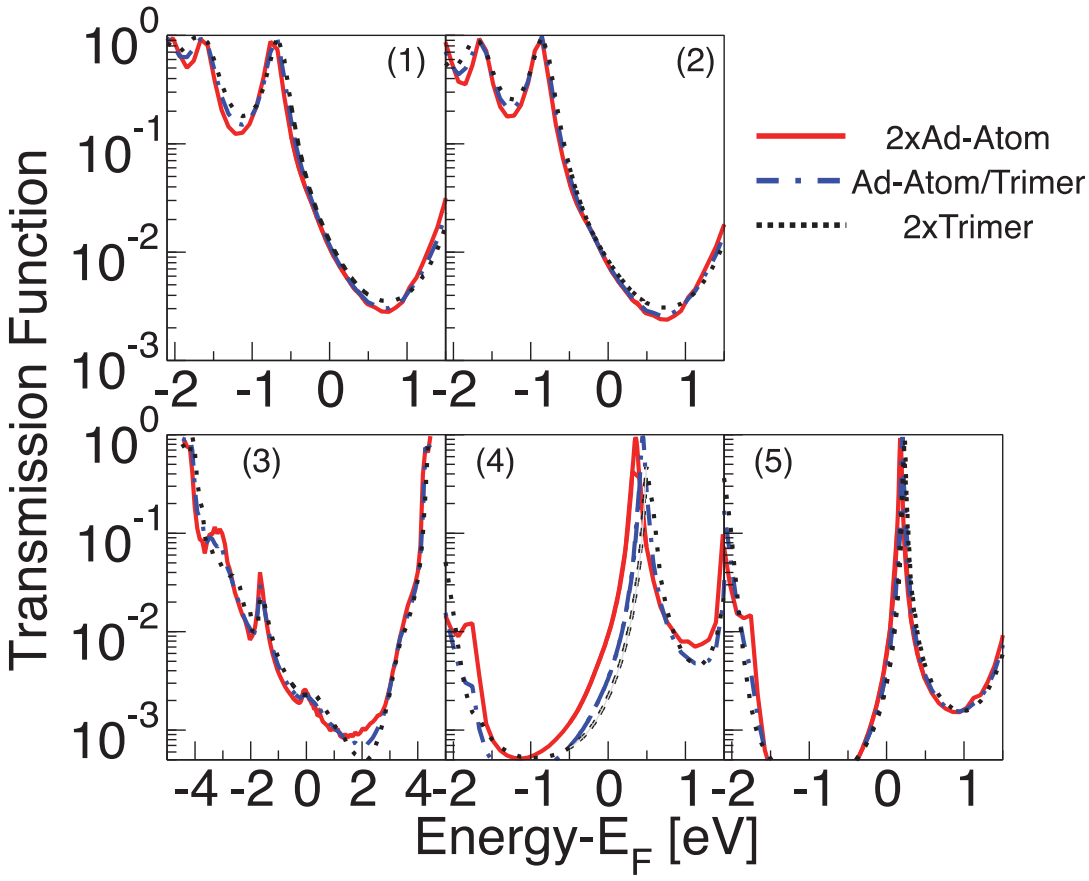

SI Figure S6: DFT transmission functions for molecules (1) to (5)

Comparison of experiments and DFT values for the conductance and Seebeck coefficient

Mol	G_{EXP} (10^{-3} G_0)	S_{EXP} (μV/K)	G_{DFT} (10^{-3} G_0)	S_{DFT} (μV/K)
(1)	0.63	13.0	11.20	25.70
(2)	0.57	9.7	7.70	20.99
(3)	0.39	1.1	2.27	1.27
(4)	0.68	-9.5	6.24	-38.17
(5)	0.24	-12.3	3.85	-76.10

Self-Energy Corrections

For the self-energy corrected results, we apply a non-self-consistent correction to the mean-field Kohn-Sham Hamiltonian that includes an "isolated molecule correction" and a static, "non-local correlation" term (see Ref. [3] for details). The isolated molecule correction is computed with the ΔSCF method from a B3LYP QChem calculation[5]. The static non-local correlation correction is approximated using an image charge model on the pseudo-charge density of the levels given by SIESTA as described in Refs. [2, 3]. The position of the image plane is calculated using the procedure of Lam and Needs[6], and is found to be 1.47Å in the vacuum with respect to the average position of the surface gold atoms.

Values of the corrections to the DFT levels in the DFT+Σ method

	(1)	(2)	(3)	(4)	(5)
Corr HOMO [eV]	-1.58	-1.64	-1.35	-2.12	-1.37
Corr LUMO [eV]	1.07	0.96	-1.19	1.20	1.27

Values of the corrections to the DFT levels in the DFT+Σ method

Position of the molecular levels in DFT+Σ

	(1)	(2)	(3)	(4)	(5)
HOMO DFT+Σ [eV]	-2.31	-2.54	-4.58	-5.52	-3.94
LUMO DFT+Σ [eV]	2.87	2.90	2.12	1.47	1.39

Energies of the molecular orbitals in DFT+Σ with respect to the Fermi level

Validity of Lorentzian Model

The knowledge of the Seebeck coefficient and conductance leads to the determination of the level positions and injection rates in a Lorentzian model of a symmetric molecule. For a Lorentzian model of a symmetric molecule, the conductance at zero bias is given by:

$$G = G_0 \frac{\Gamma^2}{\Gamma^2 + E_r^2} = G_0 T(\omega = 0)$$

where Γ is the ***average*** injection rate, E_r the energy of the resonance with respect to the Fermi energy, G_0 = 7.75 × 10^{-5} Ω^{-1} the quantum of conductance, and $T(\omega) = \frac{\Gamma^2}{\Gamma^2+(\omega-E_r)^2}$ is the dimensionless transmission function. The Seebeck coefficient S is given by:

$$S = -S_0 \frac{1}{T(\omega=0)} \frac{dT(\omega)}{d\omega}\Big|_{\omega=0} \text{ and } S = -S_0 \frac{2E_r}{\Gamma^2} T(\omega = 0),$$

where S_0 = 7.2576 eV * 10^{-6}V /K. We can then obtain the values of Γ & E_r through the following equations:

$$E_r = -2\frac{S_0}{S}\left(1 - \frac{G}{G_0}\right) \text{ and } \Gamma = \sqrt{\frac{-2GS_0E_r}{SG_0}}$$

Mol	G_{EXP} [10^{-3} G_0]	S_{EXP} [μV/K]	E_r [eV]	Γ [eV]
(1)	0.63	13.00	-1.12	0.03
(2)	0.57	9.70	-1.50	0.04
(3)	0.39	1.10	-13.19	0.26
(4)	0.68	-9.50	1.53	0.04
(5)	0.24	-12.30	1.18	0.02

Values obtained through this approach are in agreement with our explicit self-energy-corrected DFT calculations for molecules (**4**) & (**5**), consistent with the computed Lorentzian lineshape. For molecules (**1**), and (**2**), the HOMO resonance is predicted to be too close to the Fermi energy from the Lorentzian model, related to the breakdown of the Lorentzian model consecutive to the coupling with d-states of gold, also observed in molecule (**3**).

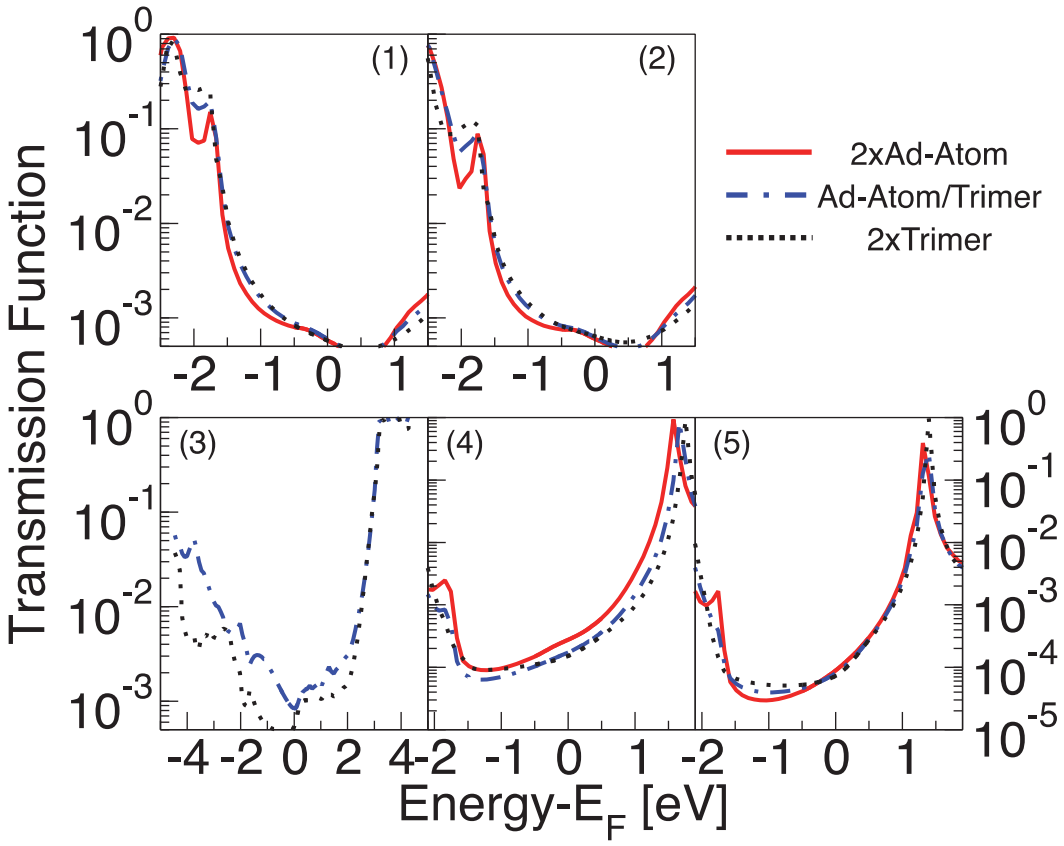

SI Figure 7: DFT+Σ transmission functions for molecules (1) to (5)

References:

1. Quek, S. Y.; Kamenetska, M.; Steigerwald, M. L.; Choi, H. J.; Louie, S. G.; Hybertsen, M. S.; Neaton, J. B.; Venkataraman, L. *Nat. Nano.,* **2009,** 4, (4), 230-234.
2. Quek, S. Y.; Venkataraman, L.; Choi, H. J.; Loule, S. G.; Hybertsen, M. S.; Neaton, J. B. *Nano Lett.,* **2007,** 7, (11), 3477-3482.
3. Quek, S. Y.; Choi, H. J.; Louie, S. G.; Neaton, J. B. *Nano Lett.,* **2009,** 9, (11), 3949-3953.
4. Choi, H. J.; Marvin, L. C.; Steven, G. L. *Phys. Rev. B,* **2007,** 76, (15), 155420.
5. Shao, Y.; Molnar, L. F.; Jung, Y.; Kussmann, J.; Ochsenfeld, C.; Brown, S. T.; Gilbert, A. T. B.; Slipchenko, L. V.; Levchenko, S. V.; O'Neill, D. P.; DiStasio Jr, R. A.; Lochan, R. C.; Wang, T.; Beran, G. J. O.; Besley, N. A.; Herbert, J. M.; Yeh Lin, C.; Van Voorhis, T.; Hung Chien, S.; Sodt, A.; Steele, R. P.; Rassolov, V. A.; Maslen, P. E.; Korambath, P. P.; Adamson, R. D.; Austin, B.; Baker, J.; Byrd, E. F. C.; Dachsel, H.; Doerksen, R. J.; Dreuw, A.; Dunietz, B. D.; Dutoi, A. D.; Furlani, T. R.; Gwaltney, S. R.; Heyden, A.; Hirata, S.; Hsu, C.-P.; Kedziora, G.; Khalliulin, R. Z.; Klunzinger, P.; Lee, A. M.; Lee, M. S.; Liang, W.; Lotan, I.; Nair, N.; Peters, B.; Proynov, E. I.; Pieniazek, P. A.; Min Rhee, Y.; Ritchie, J.; Rosta, E.; David Sherrill, C.; Simmonett, A. C.; Subotnik, J. E.; Lee Woodcock Iii, H.; Zhang, W.; Bell, A. T.; Chakraborty, A. K.; Chipman, D. M.; Keil, F. J.; Warshel, A.; Hehre, W. J.; Schaefer Iii, H. F.; Kong, J.; Krylov, A. I.; Gill, P. M. W.; Head-Gordon, M. *Phys. Chem. Chem. Phys.,* **2006,** 8, (27), 3172-3191.
6. Lam, S. C.; Needs, R. J. *J. Phys.:Cond. Mat.,* **1993,** 5, (14), 2101-2108.